



HAL
open science

Morphology of ultrathin gold and copper coatings thermally evaporated on polydimethylsiloxane elastomers: from isolated nanoparticles to continuous coatings

Julie Schweitzer, Gautier Schrodj, Alban Florentin, Emmanuel Denys, Loic Vidal, Thierry David, Francois Rouillard, Florence Bally - Le Gall, Fabrizio Spano, Vincent Roucoules, et al.

► To cite this version:

Julie Schweitzer, Gautier Schrodj, Alban Florentin, Emmanuel Denys, Loic Vidal, et al.. Morphology of ultrathin gold and copper coatings thermally evaporated on polydimethylsiloxane elastomers: from isolated nanoparticles to continuous coatings. *Thin Solid Films*, 2023, 781, pp.139972. 10.1016/j.tsf.2023.139972 . cea-04244549

HAL Id: cea-04244549

<https://cea.hal.science/cea-04244549>

Submitted on 16 Oct 2023

HAL is a multi-disciplinary open access archive for the deposit and dissemination of scientific research documents, whether they are published or not. The documents may come from teaching and research institutions in France or abroad, or from public or private research centers.

L'archive ouverte pluridisciplinaire **HAL**, est destinée au dépôt et à la diffusion de documents scientifiques de niveau recherche, publiés ou non, émanant des établissements d'enseignement et de recherche français ou étrangers, des laboratoires publics ou privés.

Morphology of ultrathin gold and copper coatings thermally evaporated on polydimethylsiloxane elastomers: from isolated nanoparticles to continuous coatings

Julie Schweitzer¹, Gautier Schrodj¹, Alban Florentin¹, Emmanuel Denys¹, Loic Vidal¹, Thierry David², François Rouillard^{3,4}, Florence Bally-Le Gall¹, Fabrizio Spano⁵, Vincent Roucoules¹, Laurent Vonna¹

¹Université de Haute-Alsace, Université de Strasbourg, CNRS, IS2M UMR 7361, 68100 Mulhouse, France

²Commissariat à l’Energie Atomique et aux Energies Alternatives, DES, ISEC, DPME, Univ. Montpellier, Marcoule, BP 17171, 30207 Bagnols sur Cèze Cedex, France

³TECHNETICS Group France, 42029 Saint-Etienne, France

⁴Laboratoire d’étanchéité maestral, 26700 Pierrelatte, France

⁵School of Engineering, Zurich University of Applied Sciences, Technikumstrasse 9, Winterthur, Switzerland

This article presents a morphological study of ultrathin gold and copper coatings (between 1 nm and 20 nm equivalent metal thickness) thermally evaporated on polydimethylsiloxane (PDMS). Results are discussed on the basis of transmission electron microscopy (TEM) and atomic force microscopy (AFM). Gold is demonstrated to grow in the form of isolated particles following a Volmer-Weber growth mode, whereas copper more likely grows in the form of a continuous film, following a Stranski–Krastanov growth mode. Our results demonstrate a negligible role of the PDMS elastic modulus (between 0.5 MPa and 2.5 MPa) in the gold and copper coatings morphology respectively. However, significant morphological changes are observed when the metals are thermally evaporated on a PDMS substrate of extremely higher surface elastic modulus obtained after O₂ plasma exposure.

INTRODUCTION

Condensation of evaporated metals on polymers leads in most cases to the growth of isolated nanoparticles due to the weak interactions between metal atoms and polymer, in comparison with the strong interactions between metal atoms. This so-called Volmer-Weber growth mode was demonstrated for example for gold, copper and silver evaporated on different types of polymeric substrates such as epoxy resins, polyimide, Teflon, polystyrene, or polycarbonate [1–4]. It appears in these studies that the chemical nature of the polymer and that of the metal strongly influence the size, morphology, and surface distribution of the growing nanoparticles. These features are also influenced by the deposition rate [5] or thermal annealing for example [6–8]. Beyond a critical thickness, particles coalesce into semi-continuous films. This thickness sets the limit between applications based on polymer-supported isolated metal nanoparticles, for instance in heterogeneous catalysis or optoelectronics [9–13], and those based on polymer-supported semi-continuous metal polymer-supported microelectronics, sensors and solar cells for example [14–16].

In the specific case of elastomeric substrates, metallic coatings were recently proposed in many applications such as flexible sensors, electronic and optical devices for example [17–23], the metallic coating being in the form of a particle-based monolayer or a continuous coating. Despite these numerous applications and unlike stiffer polymeric substrates, very few studies discuss the growth mechanism of evaporated metals on elastomeric substrates. Indeed, while most of the studies focus on the mechanical behavior and morphological evolution of elastomer-supported metal coatings thicker than tenths of nanometers [24–31], only little is known about the very first moment of the growth and the related morphology of the metallic coating on the elastomeric substrate [25]. It is however the behavior of the first atoms condensing on the substrate that defines the morphology and surface distribution of the growing nanoparticles, or the mechanical and adhesive properties of the continuous metal coating. This knowledge is crucial for the subsequent control of the required electrical, optical or mechanical properties.

In the present work, we discuss the growth mechanism of gold and copper coatings thermally evaporated on Sylgard 184 polydimethylsiloxane (PDMS) using transmission electron microscopy (TEM) and atomic force microscopy (AFM) for metal thicknesses between 1 nm and 20 nm. Sylgard 184 was chosen as model elastomer since it is very often used as elastomeric substrate in experimental studies using metal coated elastomers [25,32,33]. We have considered gold and copper for their wide range of applications, and because of their weak and strong interactions expected with polar moieties of PDMS respectively. Two distinct PDMS elastic moduli

easily achievable with the Sylgard 184 kit (0.5 MPa and 2.5 MPa) were considered in order to identify a possible role of the substrate elasticity in the morphology of metal coatings. Additionally, we considered an extremely high surface elastic modulus (in the order of 1 GPa) obtained after O₂ plasma treatment of the PDMS substrate. This surface treatment is often proposed as a convenient way to turn the surface from hydrophobic to hydrophilic. It allows grafting of functional molecules or changing liquid/surface interaction for microfluidic applications for example. The following results are discussed in the context of the growth of isolated metal nanoparticles on PDMS elastomers that is relevant for a large variety of applications.

MATERIALS AND METHODS

Elaboration of the metallized Sylgard 184 polydimethylsiloxane substrates Gold and copper (from Umicore and Thermofischer scientific respectively) were evaporated onto a thin Sylgard 184 polydimethylsiloxane film (Dow Corning, Midland, MI, United States) supported by a formvar copper mesh grid of 3 mm diameter (Agar Scientific Ltd, Stansted, United Kingdom) for TEM observations. This supported polydimethylsiloxane (PDMS) substrate was elaborated following a procedure proposed by Thangawng *et al.* [34]. The two components of the Sylgard 184 (prepolymer and cross-linker) were first mixed and degassed at ambient air during 20 min before being diluted at a concentration of 5% w/w in hexane in order to reduce the viscosity and thus, to produce thinner spin-coated films. 200 μ l of this solution was poured on the 3 mm large TEM grid already placed in the spin-coater. The film was then formed at an acceleration of 3 000 rpm² and a speed of 6000 rpm during 90 seconds. The grid covered with Sylgard 184 was then placed in an oven at 80°C during 5 hours for curing. Deposition of gold and copper was carried out using an evaporator (Auto 360 vacuum, from Edwards). The pressure was kept at $2.5 \cdot 10^{-5}$ mbar and the deposition rate was fixed at 0.1 nm s^{-1} . Distance between the sample and the metal source was fixed at 15 cm.

Characteristics of the Sylgard 184 polydimethylsiloxane (PDMS) substrates Three different surface elastic moduli were considered. The two first were obtained with prepolymer to cross-linker weight ratios of 10/1 and 10/0.5 respectively. Mechanical analyses of these samples were performed on a INSTRON 4505 dynamometer (Zwick upgraded, ZwickRoell Testing Systems GmbH, Fürstenfeld, Austria) equipped with a 1 kN force sensor, with a preload of 0.2 N and a deformation speed of $10 \text{ mm}\cdot\text{min}^{-1}$, according to the ISO 527 standard. The elastic modulus was estimated from the linear part of the stress-strain curve at small deformations and led to an elastic modulus of $2.1 \pm 0.1 \text{ MPa}$ for the ratio 10/1 and $0.4 \pm 0.1 \text{ MPa}$ for the ratio 10/0.5 respectively (the uncertainty given for the elastic modulus covers three independent measurements). The two previous PDMS substrates are named “0.5 MPa” and “2.5 MPa” in the following.

The substrate with the highest surface modulus was obtained after O₂ plasma exposure, which is commonly proposed to adjust the chemical and mechanical surface properties of PDMS. The Sylgard 184 cured at a ratio of 10/1 was exposed during 2 min to the plasma generated at 50W and $1 \cdot 10^{-2}$ mbar. As assessed by wettability measurements this exposure leads to the formation of a highly hydrophilic silica-like (SiO_x) surface, which recovers over few days the hydrophobicity of the initial PDMS due to the diffusion of free polymer chains towards the surface [35–43]. In our case, hydrophobic feature was recovered after 6 days and the sample was metallized

only then. In our experimental conditions the thickness of the silica layer is expected to be in the order of tenths of nanometer [39]. This silica-like (SiO_x) overlayer is characterized by a high elastic modulus as compared to that of the PDMS bulk material. It was shown that depending on the oxidative conditions, elastic moduli from several tens of MPa to 2 GPa can be obtained by O₂ plasma treatments [44,45]. Surface mechanical measurements were performed on a Nanoscope IV atomic force microscope (in the PeakForce QNM mode from Brücker, Billerica, Massachusetts, USA) at air and ambient conditions. Force-distance curves were acquired at 2 kHz with a cantilever of 48 N.m⁻¹ and a resonant frequency of 190 kHz. Although extremely heterogeneous, the surface elastic modulus was found to be in between 1 GPa and 10 GPa, which is in the order of magnitude of the elastic modulus expected after such treatment. We thus consider in the following that the O₂ plasma treated Sylgard 184 PDMS has a silica-like (SiO_x) overlayer with a surface elastic modulus much significantly higher than the one of non-treated PDMS. This PDMS substrate is named “1 GPa” in the following.

Observations of the metallized Sylgard 184 polydimethylsiloxane (PDMS) substrates Atomic force microscopy (AFM) imaging was performed on a Flex AFM equipped with a C3000 controller (Nanosurf, Liestal, Switzerland), with AFM probe cantilevers of 13-77 N.m⁻¹ and acquisition frequencies of 2 kHz. Transmission electron microscopy (TEM) was performed on an ARM-200F microscope (JEOL, Tokyo, Japan) working at 200 kV.

Statistical analysis of the metallized Sylgard 184 polydimethylsiloxane (PDMS) substrates TEM images were analyzed using the freeware ImageJ [46]. Particle Feret’s diameter, projected area, circularity, as well as particle surface density and covered area were calculated after thresholding TEM images. The circularity is calculated by the software using the formula $circularity = 4\pi (area/perimeter^2)$. Three independent experiments were performed for each substrate elastic modulus for reproducibility purposes. Since the distributions of the particle Feret’s diameter, projected area, circularity are not normal, the median and interquartile range values of these measurements are given in the following.

RESULTS AND DISCUSSION

Figure 1 shows transmission electron microscopy (TEM) images of Sylgard 184 coated with gold for different metal thicknesses (1 nm, 5 nm, 10 nm and 20 nm), at different magnifications. At 1 nm and 5 nm thicknesses, coatings are made of discrete nanoparticles, with circular and wormlike shapes (Figure 1A and B). Figure 2 gives for these two thicknesses, the statistics of the particle morphologies (Feret's diameter, projected area and circularity), the particle surface density and the surface coverage. Increasing the amount of condensed gold from 1 nm to 5 nm equivalent thickness leads to an increase of the median Feret's diameter (from 8.0 nm to 13.2 nm with an interquartile range (IQR) of 5.4 nm and 8.4 nm respectively), an increase of the median particle projected area (from 38 nm² to 125 nm² with an IQR of 34 nm² and 116 nm² respectively). This increase of particles size is associated to a decrease of the median circularity (from 0.88 to 0.79 with an IQR of 0.20 and 0.19), a decrease of the particle surface density (from 5 600 particles/μm² to 3 500 particles/μm²) and an increase of the surface coverage (from 22% to 37%). These trends can be explained by a spreading and coalescence of the growing particles that finally lead to a decrease of particle surface density and circularity associated to an increase of the surface coverage. It also suggests gold to grow on Sylgard 184 following a Volmer-Weber mode. This mode is commonly associated to weak interactions between the condensed atoms and the substrate that lead to atoms surface diffusion and ultimately to the growth of isolated particles as shown in Figure 1. On the whole, the morphology of the particles and their evolution during their growth are very similar to what is usually described for gold growing on polymers [2,47,48]. High magnification observations of these particles reveal remarkable ordering at the atomic scale (Figure 3A and B).

For an equivalent metal thickness of 10 nm, the coalescence of particles leads to irregular and interconnected particles, so that median Feret's diameter, median particle projected area and median circularity are difficult to measure (Figure 1C). The surface coverage increases up to 78%. With further increase in the equivalent film thickness to 20 nm, a semi-continuous film with uncovered areas similar to cracks is formed with a coverage of around 91% (Figure 1D). A TEM image of this semi-continuous film is given at smaller magnification in Figure 4A. Uncovered crack-like areas are still observed for thicker coatings, such as in 60 nm thick coatings, as illustrated in Figure 4B.

Although it was not the aim of this study, the transition between the formation of isolated particles and a percolated coating is found to occur for an equivalent metal thickness of about 10 nm. This thickness sets the limit between potential particle-based applications and semi-continuous coating-based ones.

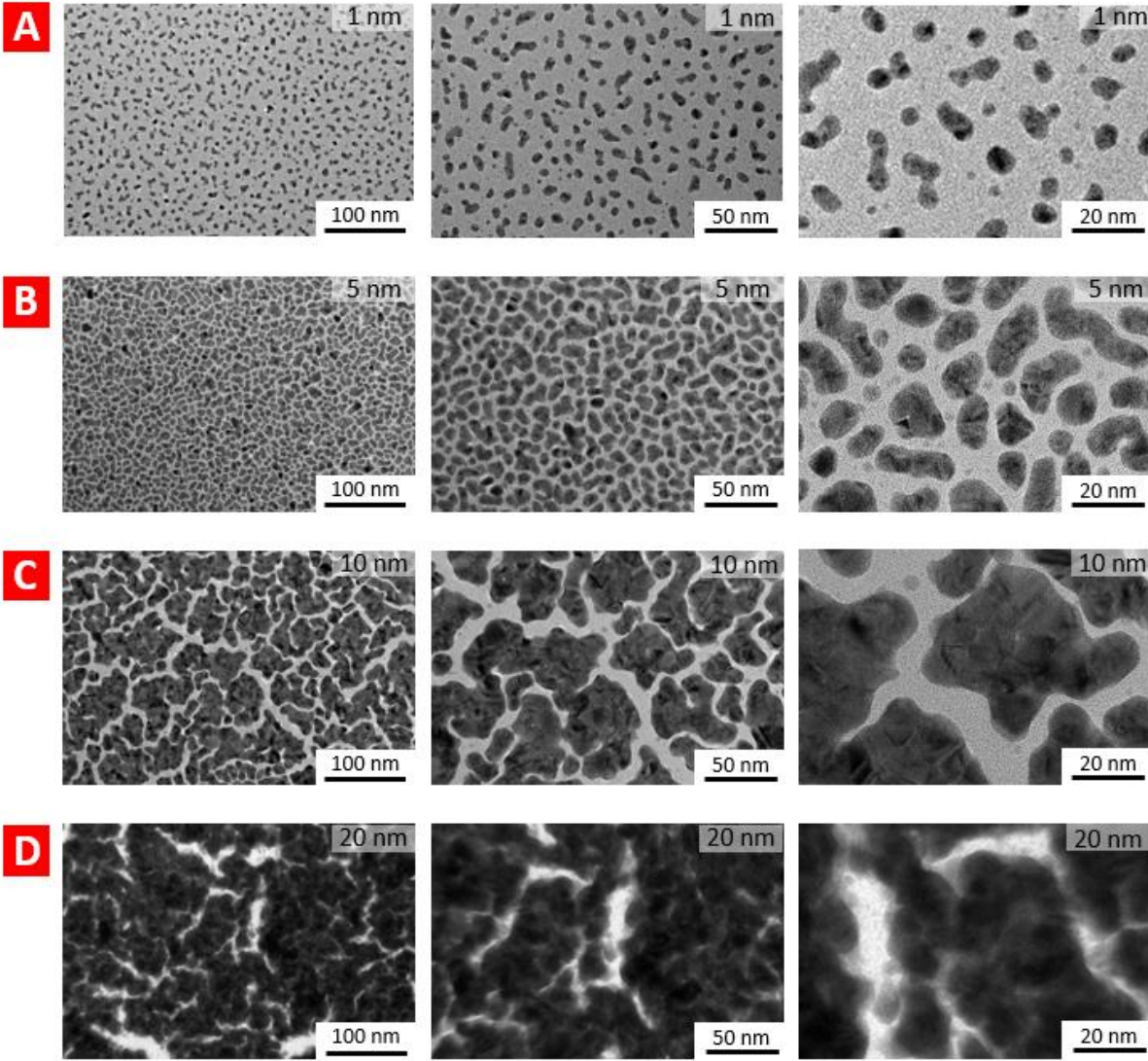
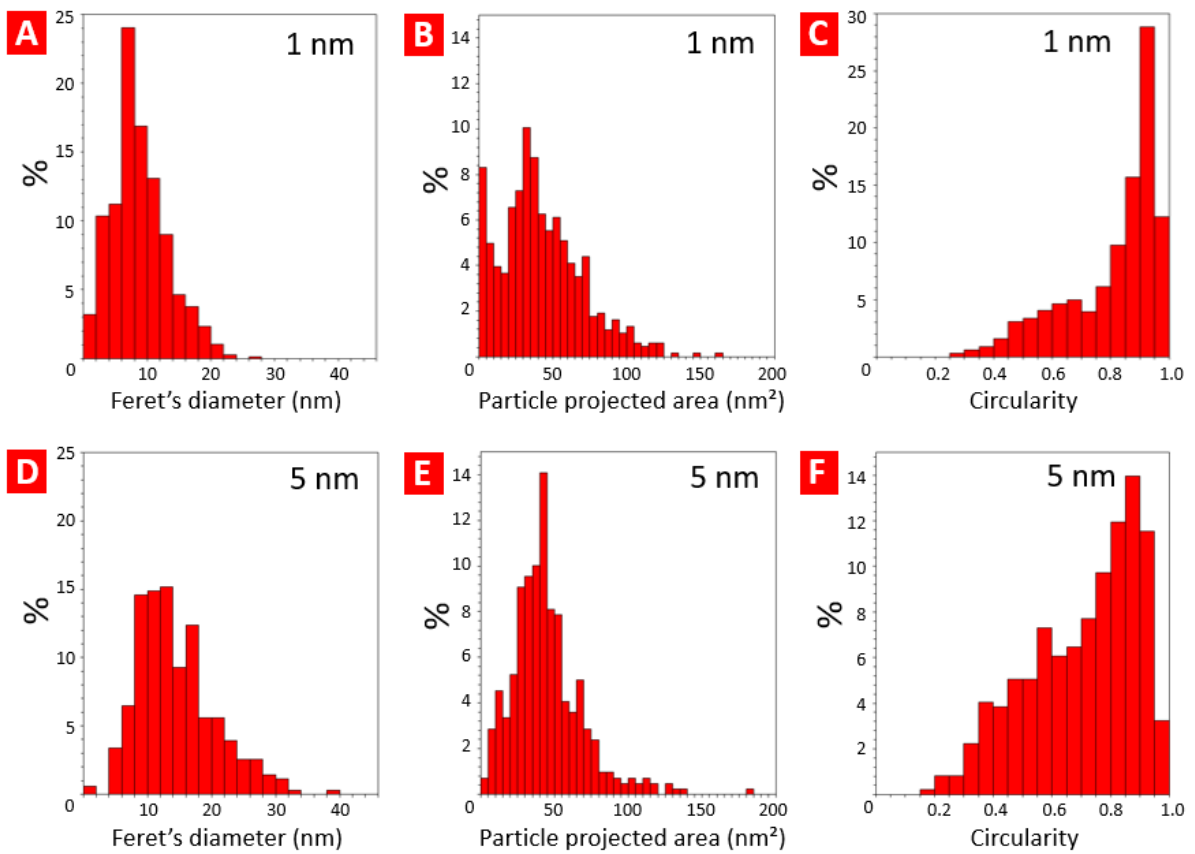


Figure 1 : TEM images at three different magnifications of Sylgard 184 coated with gold at an equivalent metal thickness of 1 nm (A), 5 nm (B), 10 nm (C) and 20 nm (D).



Sample	Feret's diameter (nm)	Particle projected area (nm ²)	Circularity	Particle surface density (μm ⁻²)	Surface coverage (%)
1 nm / 2.5 MPa	8.0 (5.4)	38 (34)	0.88 (0.20)	5 600	22
5 nm / 2.5 MPa	13.2 (8.4)	72 (68)	0.79 (0.19)	3 500	40

Figure 2 : Statistical analyses of gold particles morphologies and coverage for 2.5 MPa Sylgard 184 substrate at an equivalent metal thickness of 1 nm and 5 nm (from Figure 1A and 1B – first column): distribution in percentage of the particle Feret's diameter, projected area and circularity at 1 nm (A, B and C) and at 5 nm (D, E and F) respectively. In table, for the two thicknesses, median value extracted from the previous distributions (the number in brackets corresponds to the Interquartile Range), and values of the particle surface density and surface coverage.

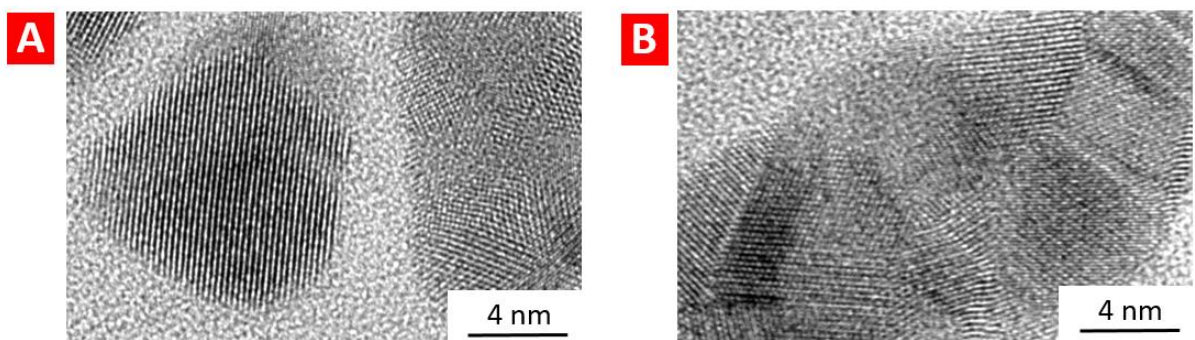


Figure 3 : TEM images at high magnification of gold particles grown on Sylgard 184 (at 5 nm equivalent thickness)

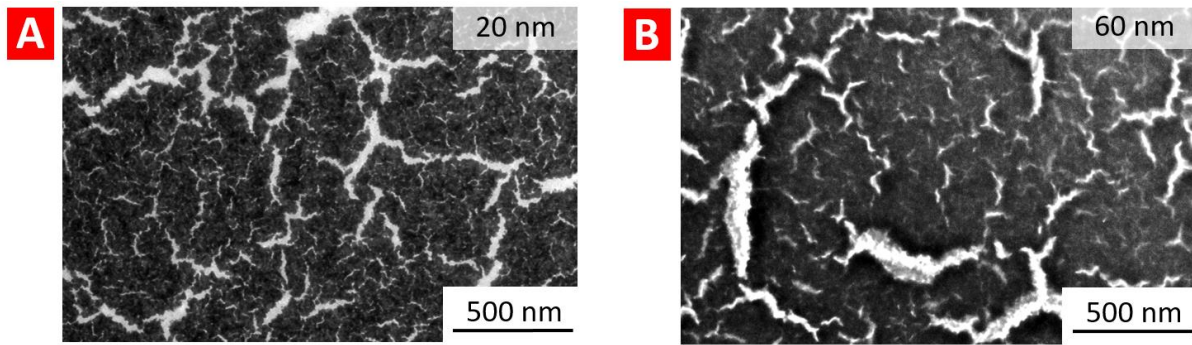


Figure 4 : TEM images of gold coatings on Sylgard 184, at a thickness of 20 nm (A) and 60 nm (B).

Figure 5 shows TEM images of Sylgard 184 coated with copper for different copper thicknesses (1 nm, 5 nm, 10 nm and 20 nm) and at different magnifications. Unlike gold, the deposition of 1 nm of copper led to a darkening of the images, without the possibility to observe particles at the surface, suggesting the growth of a continuous coating. For thicknesses from 5 nm to 10 nm (Figure 5B and Figure 5C respectively) blurry dots can be distinguished whereas contrasted particles were observed with gold at these same thicknesses (Figure 1B and Figure 1C). Finally, these dots whose size increases with increasing the amount of condensed copper turn into domains of higher contrast, with well-organized crystalline domains as assessed by the observation of Moiré patterns in the TEM images (pointed by white arrows in Figure 5D). A similar coating morphology constituted by blurry particles, as observed by TEM, was already described for copper evaporated onto polyimide [1] and epoxy resins [2]. Although the copper morphology was attributed in these studies to a Volmer-Weber growth mode, we more likely believe that the darkening of the TEM image at 1 nm of deposition and the subsequent growth of blurry dots corresponds to a Stransky-Krastanov growth mode. Indeed, this growth mode is characterized by a growth initiation in the form of a 2D layer followed by the growth of 3D islands over a continuous metal layer. The oxygen rich polydimethylsiloxane backbone of Sylgard 184 can indeed strongly interact with copper atoms that condense on the elastomer surface. We measured in a previous study the interaction of copper condensed on silicon oxide, which could be considered as a relatively close oxygenated substrate, and we reported remarkably high adhesive force [49]. A strong interaction between copper and different polymers (polystyrene, polyvinyl alcohol, polyethylene oxide, polyvinyl methyl ether, polyvinyl acetate, and polymethyl methacrylate) through the formation of an oxygen rich interphase is also assessed since decades [50]. In the case of polydimethylsiloxane surfaces, stronger adhesion of a copper coatings was also observed after Ar^+ ion irradiation due to the etching of free chains and to the enrichment of the elastomer surface

in oxygen species [51]. More recently, copper condensing on epoxy resins was shown to interact preferentially with Cu atoms and hydroxyls to form Cu–O–C bonds [52].

The hypothesis of a Stransky-Krastanov growth mode in the case of copper is supported by atomic force microscopy (AFM) observations of 20 nm thick metal coatings on Sylgard 184. Figure 6 shows typical topographic AFM images of these coatings. Topographic image of the gold coating (Figure 6A) shows a granular structure corresponding to the granular domains observed on the TEM images (Figure 1D). The surface is relatively smooth, with a full height scale at 20 nm. Unlike gold, the topographic image of the copper coating (Figure 6B) shows relatively large and high wrinkles (height scale is in this case 380 nm). It was shown that these wrinkles arise from the differential elastic properties between the metallic coatings and the elastic substrate [53]. It supposes a continuous and adhering coating that transmit the mechanical constraint at the origin of the surface deformation into wrinkles. This observation supports in our case the hypothesis of a continuous and adhering copper film. Similar wrinkles were indeed observed for metals strongly adhering to the elastomer substrate as for example for chromium sputtered on Sylgard 184 at thicknesses between 8 nm and 15 nm. [25]. However, the sparse and isolated particles of gold resulting from the lower metal/elastomer interactions as compared to copper, do not transmit such a constraint and no wrinkle is observed in this case (Figure 6A). The absence of wrinkles for such thin gold coatings agrees with observations already discussed in the literature, as in the case of gold sputtered on Sylgard 184 at thicknesses between 8 nm and 24 nm [25].

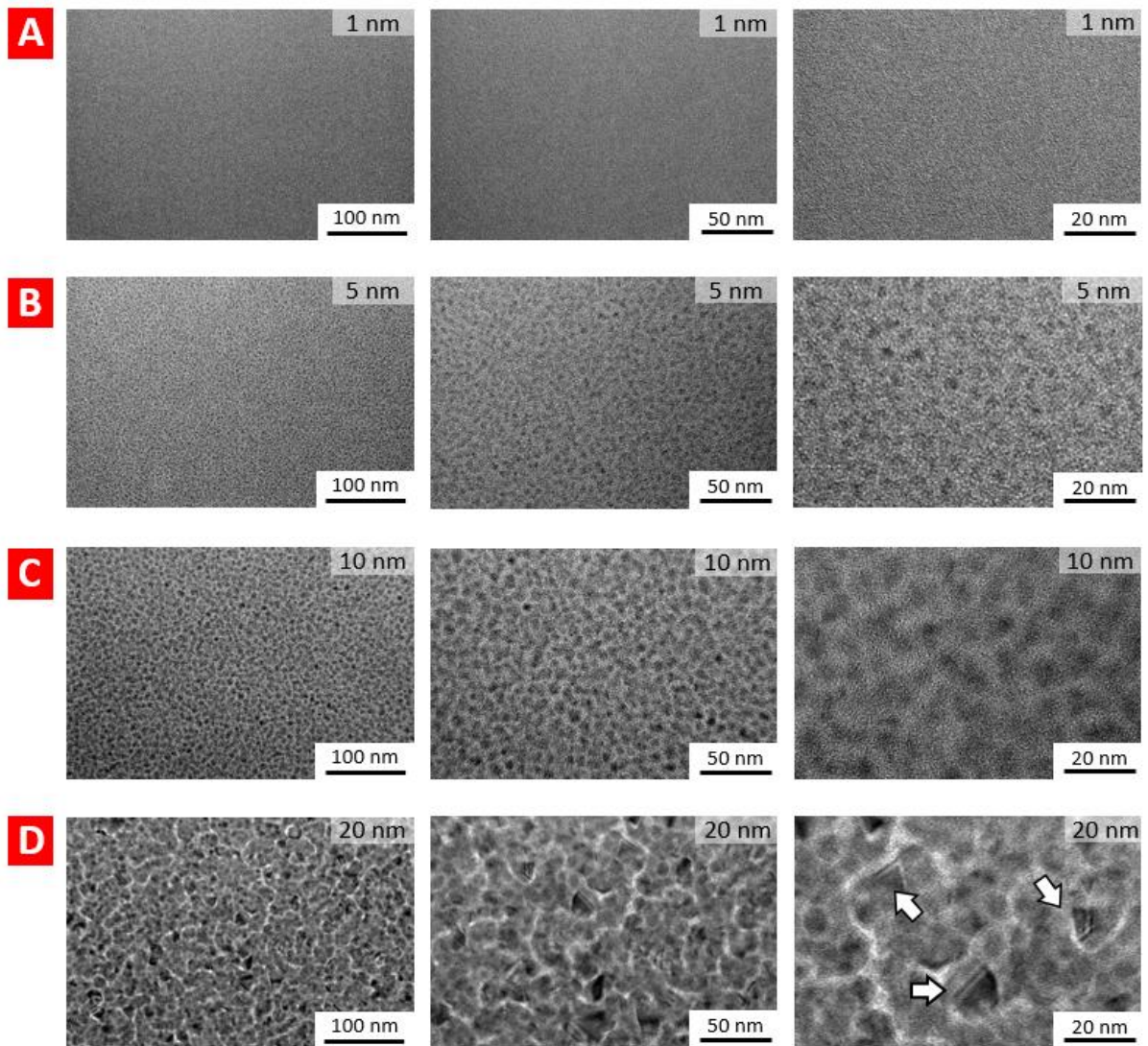


Figure 5 : TEM images of Sylgard 184 coated with copper at a thickness of 1 nm (A), 5 nm (B), 10 nm (C) and 20 nm (D), at three different magnifications.

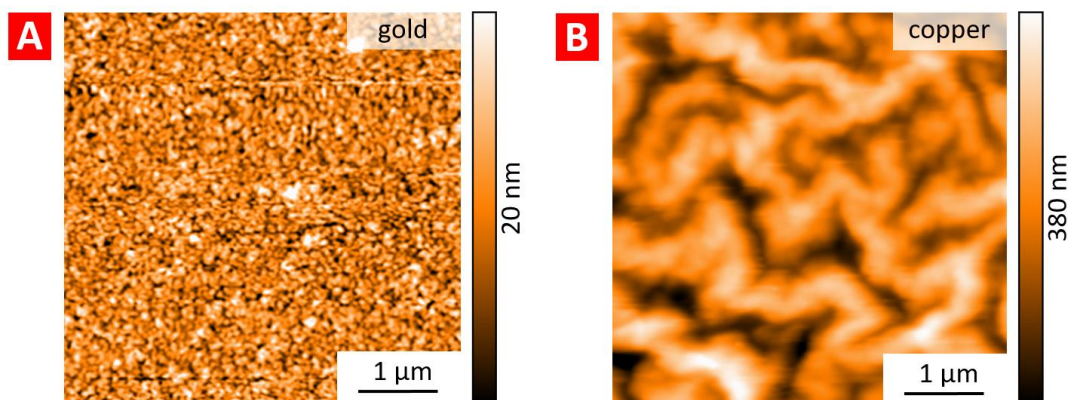


Figure 6 : Topographic AFM images of 20 nm thick gold (A) and copper (B) coatings on Sylgard 184.

To study the effect of the elastic modulus on the morphology of growing gold and copper coatings on Sylgard 184, we studied two other elastic moduli in addition to the commonly used 2.5 MPa Sylgard 184: (i) a low elastic modulus, of 0.5 MPa, corresponding to the lowest elastic modulus obtained by reducing the cross-linker/base ratio of the Sylgard 184 kit, and (ii) an extremely high surface elastic modulus, in the order of 1 GPa, obtained after O₂ plasma exposure, that is commonly used as a technique for mechanical and chemical surface modification of Sylgard 184 (see experimental section). Figure 7 shows characteristic TEM images of Sylgard 184 of different surface elastic moduli (0.5 MPa, 2.5 MPa and 1 GPa) coated with gold at three different equivalent metal thicknesses (1 nm, 5 nm and 10 nm).

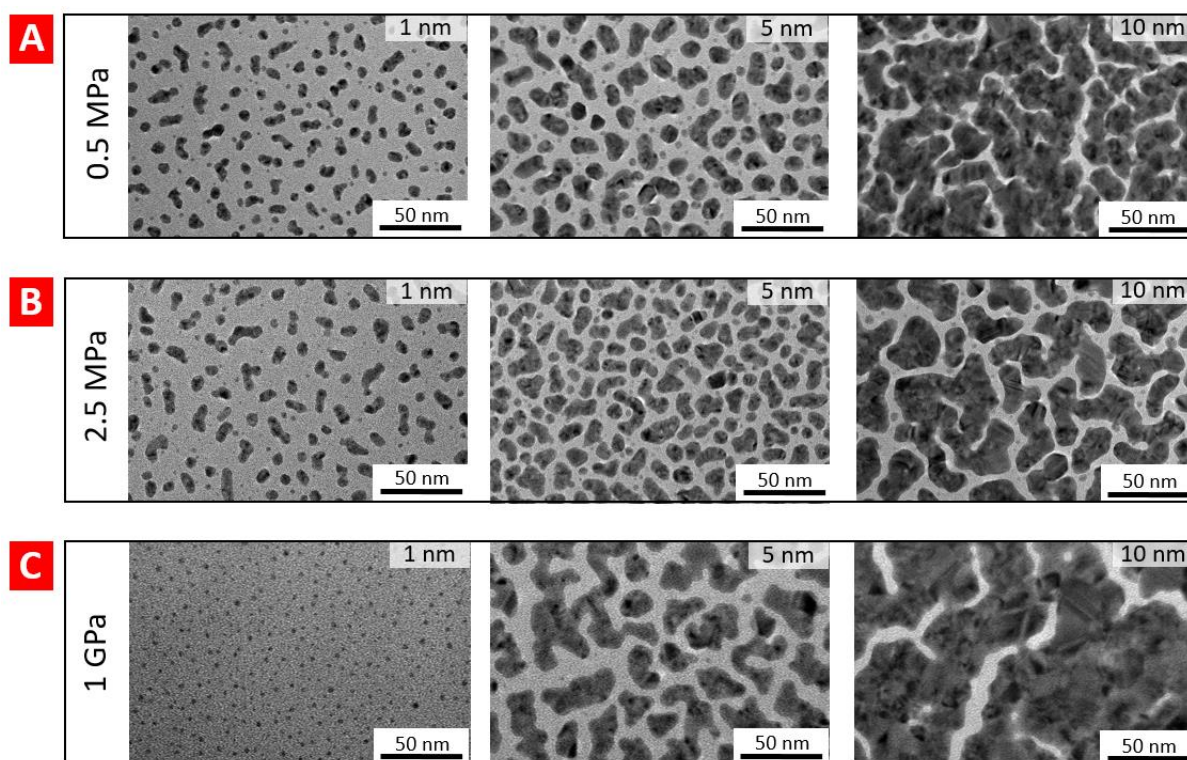
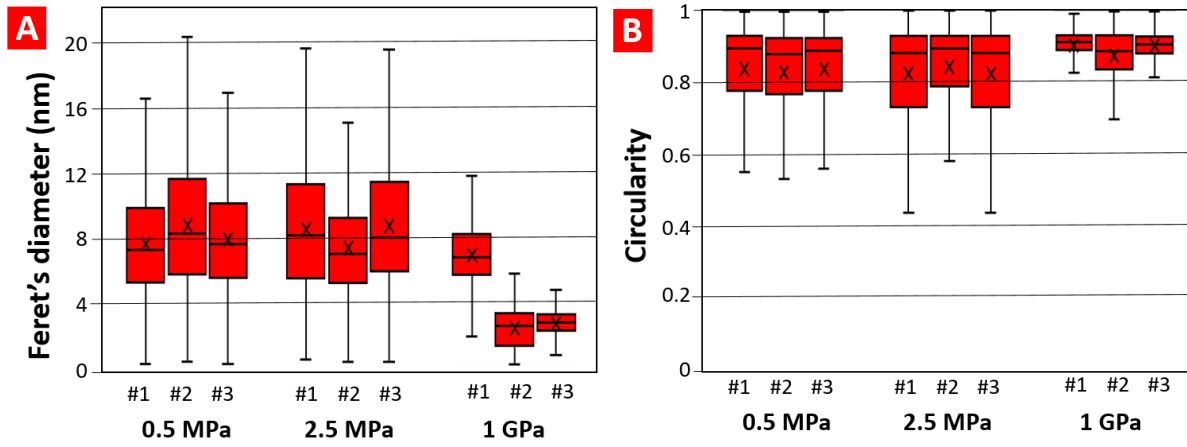


Figure 7 : TEM images of Sylgard 184 covered with gold of 1 nm, 5 nm and 10 nm metal thickness at three different surface elastic moduli: (A) 0.5 MPa, (B) 2.5 MPa and (C) 1 GPa obtained after O₂ plasma exposure.

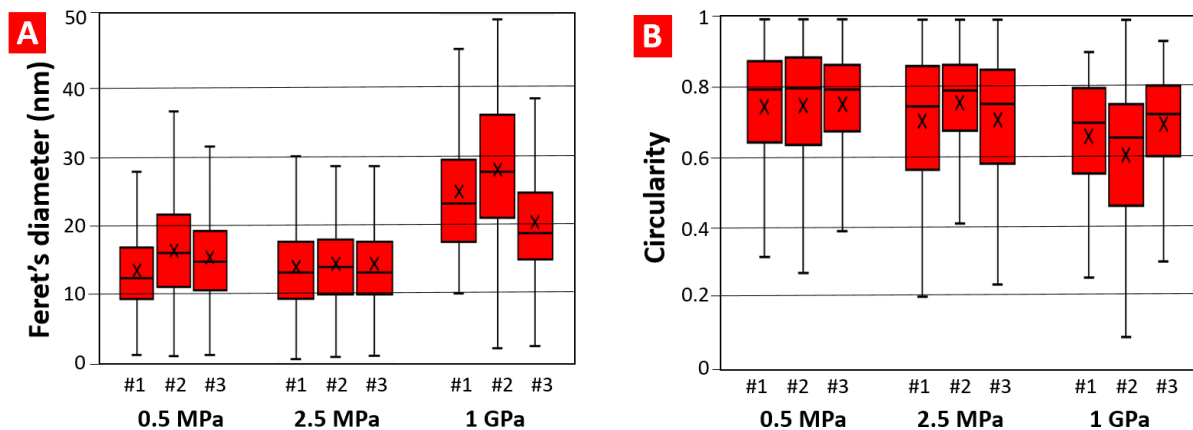
Figure 8 and Figure 9 give the statistical analyses of the gold particles features and the corresponding coatings grown on Sylgard 184 of different elastic moduli for equivalent metal thicknesses of 1 nm and 5 nm respectively. These data are provided for three independent experiments for reproducibility purposes. At a given elastic modulus, these results confirm the general trend of an increase of the particle size, decrease of circularity and particle surface density, when increasing the thickness (table in Figure 8 and Figure 9) as discussed earlier (table in Figure 2). For an equivalent thickness of 1 nm, no significant difference in the particle size and circularity can be observed for the three different elastic moduli (Figure 8A and B). Smaller particles were observed in two

independent experiments when grown on Sylgard 184 of 1 GPa (#2 and #3 in Figure 8A). However, these two experiments with small particles are also associated to low coverages which can reasonably be attributed to a lower amount of condensed gold. To our sense, this result is to be attributed to the lack of precision in the quantity of condensed metal for such small metal amount and such deposition rate. The median value of particles circularity is similar for the three modules although the distribution of the particles grown on the 1 GPa substrate is narrower. For an equivalent thickness of 5 nm, larger particles are systematically observed in the three independent experiments when grown on Sylgard 184 of 1 GPa, as compared to those grown on substrates of 0.5 and 2.5 MPa (Figure 9A). Similarly, for this elastic modulus, circularity decreases in the three independent experiments, as well as particle surface density. For an equivalent thickness of 10 nm the particle surface coverage significantly increases in the case of the 1 GPa Sylgard 184, with relatively larger gold domains, as qualitatively observed in Figure 7C.



Sample		Feret's diameter (nm)	Particle projected area (nm ²)	Circularity	Particle surface density (μm ²)	Surface coverage (%)
1 nm / 0.5 MPa	# 1	7.2 (4.5)	34 (33)	0.89 (0.15)	7 190	23
	# 2	8.2 (5.8)	37 (37)	0.88 (0.16)	5 630	24
	# 3	7.6 (4.5)	34 (28)	0.89 (0.15)	7 690	26
1 nm / 2.5 MPa	# 1	7.1 (9.5)	33 (26)	0.88 (0.14)	7 650	23
	# 2	8.1 (4.0)	42 (34)	0.89 (0.20)	6 540	27
	# 3	8.2 (5.4)	39 (36)	0.88 (0.20)	5 600	22
1 nm / 1 GPa	# 1	6.7 (2.4)	26 (16)	0.91 (0.04)	9 710	28
	# 2	2.5 (1.9)	4 (4)	0.88 (0.09)	20 900	8
	# 3	2.7 (1.0)	3 (4)	0.91 (0.05)	19 740	8

Figure 8 : Statistical analyses of gold particles morphologies grown on Sylgard 184 of three different elastic moduli, for a metal thickness of 1 nm and three independent experiments (#1, #2, #3): distribution in percentage of the particle Feret's diameter and circularity (A, B). In table, for the three elastic moduli, median value of the particle Feret's diameter, projected area and circularity (the number in brackets corresponds to the interquartile range), and values of the particle surface density and surface coverage, for the three independent experiments.



Sample		Feret's diameter (nm)	Particle projected area (nm ²)	Circularity	Particle surface density (μm ⁻²)	Surface coverage (%)
5 nm / 0.5 MPa	# 1	12 (7)	107 (97)	0.79 (0.23)	4 180	34
	# 2	16 (10)	110 (95)	0.80 (0.25)	3 266	44
	# 3	15 (8)	109 (99)	0.80 (0.19)	3 390	39
5 nm / 2.5 MPa	# 1	13 (8)	72 (68)	0.79 (0.19)	3 500	40
	# 2	14 (8)	93 (87)	0.75 (0.30)	4 700	37
	# 3	13 (7)	78 (66)	0.76 (0.27)	3 390	30
5 nm / 1 GPa	# 1	23 (12)	275 (210)	0.70 (0.25)	1 630	44
	# 2	28 (15)	325 (350)	0.66 (0.29)	690	36
	# 3	19 (10)	163 (113)	0.73 (0.20)	2 200	41

Figure 9 : Statistical analyses of gold particles morphologies grown on Sylgard 184 of three different elastic moduli, for a metal thickness of 5 nm and three independent experiments (#1, #2, #3) : distribution in percentage of the particle Feret's diameter and circularity (A, B). In table, for the three elastic moduli, median value of the particle Feret's diameter, projected area and circularity (the number in brackets corresponds to the interquartile range), and values of the particle surface density and surface coverage, for the three independent experiments.

Figure 10 shows TEM images of Sylgard 184 of different surface elastic moduli (0.5 MPa, 2.5 MPa and 1 GPa) coated with copper at three different thicknesses (1 nm, 5 nm and 10 nm). As observed with gold, lowering the elastic modulus of Sylgard 184 to 0.5 MPa does not lead to significant changes in the morphology of the growing copper coatings. For an elastic modulus of 1 GPa however, the morphology of the copper coatings (Figure 10C) differs from that observed for lower moduli. The most significant difference with the two lowest elastic moduli appears for a thickness of 10 nm for which the coating appears more homogeneous with well-organized crystalline domains as assessed by moiré patterns (pointed by white arrows in Figure 10C).

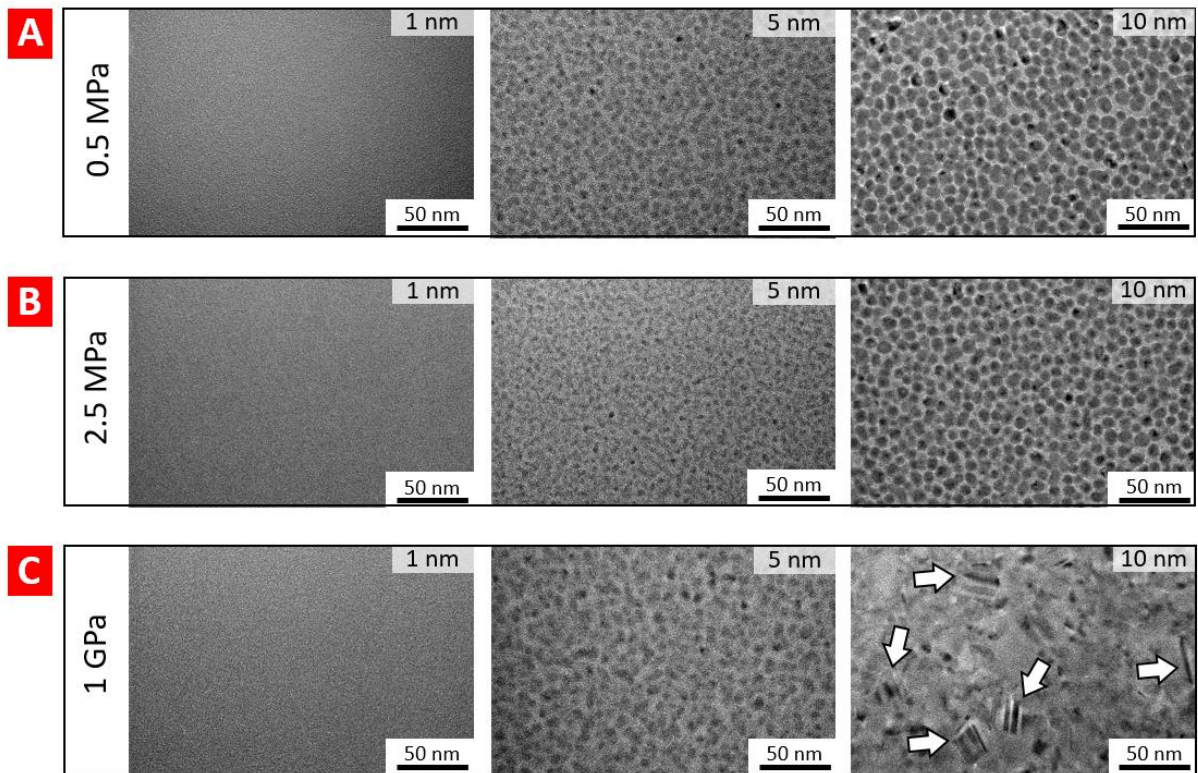


Figure 10 : TEM images of Sylgard 184 covered with copper of 1 nm, 5 nm and 10 nm metal thickness at three different surface elastic moduli: (A) 0.5 MPa, (B) 2.5 MPa and (C) 1 GPa obtained after O₂ plasma exposure.

Varying the elastic modulus of the Sylgard 184 substrate from 0.5 MPa to 2.5 MPa did not significantly change the morphology of the gold or copper coating. On the contrary, increasing the surface elastic modulus up to 1 GPa after O₂ plasma exposure led to a new coating morphology. This result might be attributed to a modification of the atom surface diffusivity due to the presence of the hard and stiff silica-like outermost layer (produced by O₂ plasma exposure). Many parameters govern the surface diffusivity of a metallic atom that adsorbs on a polymeric surface. It was shown that this diffusivity can be affected by the nature of the evaporated metal [1–3,54] and by the nature or surface energy of the polymer [1,3,4,55,56]. Also, low density polymers can lead to diffusion of metal atoms and condensation of atom clusters into the polymer substrate. Experimental evidence of this diffusion was given for example in the case of gold condensing on polycarbonate [57] and of copper on polyimide [58]. Kovacs *et al.* demonstrated that decreasing the surface energy increases the diffusion into the polymer [59]. The diffusivity being related to the specific properties of polymers, other studies evidenced an increase of diffusivity when annealing the substrate during or after deposition, eventually close to the glass transition [6–8]. This diffusion was shown to be hindered chemically and mechanically by an ultrathin chromium layer previously deposited on a polymer [60]. Similarly, we hypothesize that the hard silica-like layer resulting from the O₂ plasma exposure induces an increase of the atom surface diffusivity and thus larger gold domains.

On the contrary a possible diffusion within the elastomer for lower surface elastic modulus led to an anchoring of metal atoms in the substrate and thus to a smaller but more numerous domains.

CONCLUSION

In summary, we have examined on the basis of transmission electron microscopy and atomic force microscopy images, the morphology of gold and copper coatings thermally evaporated on Sylgard 184 polydimethylsiloxane at the very first moments of condensation and coating growth, for equivalent metal thicknesses going from 1 nm to 20 nm. Whereas gold appears clearly to grow in the form of isolated particles following a Volmer-Weber growth mode, we propose that copper more likely grows in the form of a continuous film, following a Stranski–Krastanov growth mode. Varying the Sylgard 184 elastic modulus from 2.5 MPa to the lowest achievable elastic modulus of 0.5 MPa, did not significantly changed the morphology of the gold and copper coatings respectively. However, O₂ plasma exposure often proposed for this material remarkably affects the morphology of both gold and copper coatings. We attributed these changes to the presence of a silica-like layer of extremely higher elastic modulus produced during this surface treatment, that might affect the mobility of the metal atoms and subsequently the coating growth.

Our results demonstrate the possibility of easily decorating elastomers with gold nanoparticles, reasonably of up to around 20 nm Feret's diameter. The precise control of the size, and especially for lower sizes, require a precise control of both deposition rate and amount of deposited metal. The deposition of around 10 nm equivalent thickness and above led to particles coalescence, resulting in extremely irregular and elongated shapes (ginger-like shape). However, in the case of copper, isolated particles couldn't be clearly identified, similarly to those observed for gold; the coating homogeneously covering the substrate. These two distinct morphologies, of discontinuous or continuous ultrathin metal coatings might finally give insights in the physical behaviors of thicker coatings (adhesion and cohesion for example) that are known to be governed by the microstructure of the coatings at interfaces.

ACKNOWLEDGMENTS

This work was proposed and funded by the Commissariat à l’Energie Atomique et aux Energies Alternatives (CEA) and TECHNETICS Group France (Contract CNRS131640). As part of the ITI 2021-2028 program of the University of Strasbourg, CNRS and INSERM UMR 1121, this work of the Interdisciplinary Thematic Institute HiFunMat was also supported by IdEx Unistra (ANR-10-IDEX-0002) and SFRI (STRAT’US project, ANR-20-SFRI-0012) under the framework of the French Investments for the Future Program.

1. Zaporojtchenko, V.; Behnke, K.; Thran, A.; Strunskus, T.; Faupel, F. Condensation coefficients and initial stages of growth for noble metals deposited onto chemically different polymer surfaces. *Appl. Surf. Sci.* **1999**, *144–145*, 355–359, doi:10.1016/S0169-4332(98)00826-5.
2. Kanzow, J.; Horn, P.S.; Kirschmann, M.; Zaporojtchenko, V.; Dolgner, K.; Faupel, F.; Wehlack, C.; Possart, W. Formation of a metal/epoxy resin interface. *Appl. Surf. Sci.* **2005**, *239*, 227–236, doi:10.1016/j.apsusc.2004.05.239.
3. Zaporojtchenko, V.; Zekonyte, J.; Biswas, A.; Faupel, F. Controlled growth of nano-size metal clusters on polymers by using VPD method. *Surf. Sci.* **2003**, *532–535*, 300–305, doi:10.1016/S0039-6028(03)00128-6.
4. Smithson, R.L.W.; McClure, D.J.; Evans, D.F. Effects of polymer substrate surface energy on nucleation and growth of evaporated gold films. *Thin Solid Films* **1997**, *307*, 110–112, doi:10.1016/S0040-6090(97)00310-6.
5. Haidara, H.; Papirer, Y.; Vallat, M.F.; Schultz, J. Relationships between structural properties of vapour-deposited metallic films on to polymer and their relevant adhesive performance. *J. Mater. Sci.* **1993**, *28*, 3243–3246, doi:10.1007/BF00354242.
6. Erichsen, J.; Kanzow, J.; Schürmann, U.; Dolgner, K.; Günther-Schade, K.; Strunskus, T.; Zaporojtchenko, V.; Faupel, F. Investigation of the Surface Glass Transition Temperature by Embedding of Noble Metal Nanoclusters into Monodisperse Polystyrenes. *Macromolecules* **2004**, *37*, 1831–1838, doi:10.1021/ma0353080.
7. Zaporojtchenko, V.; Strunskus, T.; Erichsen, J.; Faupel, F. Embedding of Noble Metal Nanoclusters into Polymers as a Potential Probe of the Surface Glass Transition. *Macromolecules* **2001**, *34*, 1125–1127.
8. Takele, H.; Kulkarni, A.; Jebril, S.; Chakravadhanula, V.S.K.; Hanisch, C.; Strunskus, T.; Zaporojtchenko, V.; Faupel, F. Plasmonic properties of vapour-deposited polymer composites containing Ag nanoparticles and their changes upon annealing. *J. Phys. D. Appl. Phys.* **2008**, *41*, doi:10.1088/0022-3727/41/12/125409.
9. Walter, H.; Bauer, G.; Domnick, R.; Jakopic, G.; Leitner, A. Role of granular structure in metal layers on the optical properties of absorbing mirrors. *Opt. Eng.* **2006**, *45*, 103801.
10. Bauer, G.; Hassmann, J.; Walter, H.; Haglmüller, J.; Mayer, C.; Schalkhammer, T. Nanotechnology Resonant nanocluster technology—from optical coding and high quality security features to biochips. *Nanotechnology* **2003**, *14*, 1289.
11. Guler, U.; Turan, R. Effect of Particle Properties and Light Polarization on the Plasmonic Resonances in Metallic Nanoparticles. *Opt. Express* **2010**, *18*, 17322–17338.
12. Wu, J.-L.; Chen, F.-C.; Hsiao, Y.-S.; Chien, F.-C.; Chen, P.; Chun-Hong, K.; Huang, M.H.; Hsu, C.-S. Surface Plasmonic Effects of Metallic Nanoparticles on the Performance of Polymer Bulk Heterojunction. *ACS Nano* **2011**, *5*, 959–967.
13. Schwartzkopf, M.; Santoro, G.; Brett, C.J.; Rothkirch, A.; Polonskyi, O.; Hinz, A.; Metwalli, E.; Yao, Y.; Strunskus, T.; Faupel, F.; et al. Real-Time Monitoring of Morphology and Optical Properties during Sputter Deposition for Tailoring Metal – Polymer Interfaces. *Appl. Mater. Interfaces* **2015**, *7*, 13547–13556, doi:10.1021/acsami.5b02901.
14. Cordill, M.J.; Kreiml, P.; Mitterer, C. Materials Engineering for Flexible Metallic Thin Film Applications. *Materials (Basel)*. **2022**, *15*, 1–25.
15. Girtan, M.; Negulescu, B. Optical Materials : X A review on oxide / metal / oxide thin films on flexible substrates as electrodes for organic and perovskite solar cells. *Opt. Mater. X* **2022**, *13*,

- 100122, doi:10.1016/j.omx.2021.100122.
16. Elanjeitsenni, V.P.; Vadivu, K.S.; Prasanth, B.M. A review on thin films , conducting polymers as sensor devices. *Mater. Res. Express* **2022**, 022001.
 17. Polavarapu, L.; Liz-Marzán, L.M. Towards low-cost flexible substrates for nanoplasmonic sensing. *Phys. Chem. Chem. Phys.* **2013**, *15*, 5288–5300, doi:10.1039/c2cp43642f.
 18. Lamberti, A.; Virga, A.; Rivolo, P.; Angelini, A.; Giorgis, F. Easy Tuning of Surface and Optical Properties of PDMS Decorated by Ag Nanoparticles. *J. Phys. Chem. B* **2015**, *119*, 8194–8200, doi:10.1021/acs.jpcc.5b02581.
 19. Segev-Bar, M.; Haick, H. Flexible sensors based on nanoparticles. *ACS Nano* **2013**, *7*, 8366–8378, doi:10.1021/nn402728g.
 20. Yang, X.; Zhang, M. Review of flexible microelectromechanical system sensors and devices. *Nanotechnol. Precis. Eng.* **2021**, *4*, doi:10.1063/1.5004301.
 21. Melzer, M.; Makarov, D.; Schmidt, O.G. A review on stretchable magnetic field sensorics. *J. Phys. D. Appl. Phys.* **2020**, *53*, doi:10.1088/1361-6463/ab52cf.
 22. Yu, C.; O'Brien, K.; Zhang, Y.-H.; Yu, H.; Jiang, H. Tunable optical gratings based on buckled nanoscale thin films on transparent elastomeric substrates. *Appl. Phys. Lett.* **2010**, *96*, 041111.
 23. Qi, D.; Zhang, K.; Tian, G.; Jiang, B.; Huang, Y. Stretchable Electronics Based on PDMS Substrates. *Adv. Mater.* **2021**, *33*, 1–25, doi:10.1002/adma.202003155.
 24. Graudejus, O.; Görrn, P.; Wagner, S. Controlling the morphology of gold films on poly(dimethylsiloxane). *ACS Appl. Mater. Interfaces* **2010**, *2*, 1927–1933, doi:10.1021/am1002537.
 25. Shao, Y.; Brook, M.A. Structured metal films on silicone elastomers. *J. Mater. Chem.* **2010**, *20*, 8548–8556, doi:10.1039/c0jm00824a.
 26. Arafat, Y.; Dutta, I.; Panata, R. On the deformation mechanisms and electrical behavior of highly stretchable metallic interconnects on elastomer substrates. *J. Appl. Phys.* **2016**, *120*, 11510, 11510.
 27. Polywka, A.; Stegers, L.; Krauledat, O.; Riedl, T.; Jakob, T.; Görrn, P. Controlled mechanical cracking of metal films deposited on polydimethylsiloxane (PDMS). *Nanomaterials* **2016**, *6*, 1–10, doi:10.3390/nano6090168.
 28. Bowden, N.; Brittain, S.; Evans, A.G.; Hutchinson, J.W.; Whitesides, G.M. Spontaneous formation of ordered structures in thin films of metals supported on an elastomeric polymer. *Nature* **1998**, *393*, 146–149, doi:10.1038/30193.
 29. Vandeparre, H.; Liu, Q.; Mineev, I.R.; Suo, Z.; Lacour, S.P. Localization of folds and cracks in thin metal films coated on flexible elastomer foams. *Adv. Mater.* **2013**, *25*, 3117–3121, doi:10.1002/adma.201300587.
 30. Robinson, A.P.; Mineev, I.; Graz, I.M.; Lacour, S.P. Microstructured silicone substrate for printable and stretchable metallic films. *Langmuir* **2011**, *27*, 4279–4284, doi:10.1021/la103213n.
 31. Begley, M.R.; Scott, O.N.; Utz, M.; Bart-Smith, H. Fracture of nanoscale copper films on elastomer substrates. *Appl. Phys. Lett.* **2009**, *95*, doi:10.1063/1.3268458.
 32. Béfahy, S.; Yunus, S.; Burguet, V.; Heine, J.-S.; Troosters, M.; Bertrand, P. Stretchable Gold Tracks on Flat Polydimethylsiloxane (PDMS) Rubber Substrate. *J. Adhes.* **2008**, *84*, 231–239.
 33. Lacour, S.; Suo, Z. Stretchable gold conductors on elastomeric substrates Stretchable gold conductors on elastomeric substrates. *Appl. Phys. Lett.* **2003**, doi:10.1063/1.1565683.

34. Thangawng, A.L.; Ruoff, R.S.; Swartz, M.A.; Glucksberg, M.R. An ultra-thin PDMS membrane as a bio/micro-nano interface: Fabrication and characterization. *Biomed. Microdevices* **2007**, *9*, 587–595, doi:10.1007/s10544-007-9070-6.
35. Bacharouche, J.; Haidara, H.; Kunemann, P.; Vallat, M.F.; Roucoules, V. Singularities in hydrophobic recovery of plasma treated polydimethylsiloxane surfaces under non-contaminant atmosphere. *Sensors Actuators, A Phys.* **2013**, *197*, 25–29, doi:10.1016/j.sna.2013.04.003.
36. Fritz, J.L.; Owen, M.J. Hydrophobic Recovery of Plasma-Treated Polydimethylsiloxane. *J. Adhes.* **1995**, *54*, 33–45.
37. Hillborg, H.; Sandelin, M.; Gedde, U.W. Hydrophobic recovery of polydimethylsiloxane after exposure to partial discharges as a function of crosslink density. *Polymer (Guildf)*. **2001**, *42*, 7349–7362, doi:10.1016/S0032-3861(01)00202-6.
38. Williams, R.L.; Wilson, D.J.; Rhodes, N.P. Stability of plasma-treated silicone rubber and its influence on the interfacial aspects of blood compatibility. *Biomaterials* **2004**, *25*, 4659–4673, doi:10.1016/j.biomaterials.2003.12.010.
39. Wang, Z.; Luo, Y.; Zheng, F.; Zhang, N.; Yin, C.; Li, J.; He, C.; Peng, X.; Huang, Z.; Fang, P. Study on surface structure of plasma-treated polydimethylsiloxane (PDMS) elastomer by slow positron beam. *Surf. Interface Anal.* **2018**, *50*, 819–826, doi:10.1002/sia.6484.
40. Kim, J.; Chaudhury, M.; Owen, M. Hydrophobicity loss and recovery of silicone HV insulation. *IEEE Trans Dielectr Electr Insul* **1995**, *6*, 695–702.
41. Tóth, A.; Bertóti, I.; Blazsó, M.; Bánhegyi, G.; Bogнар, A.; Szaplóczay, P. Oxidative damage and recovery of silicone rubber surfaces. 1. X-ray photoelectron spectroscopic study. *J. Appl. Polym. Sci.* **1994**, *52*, 1293–1307.
42. Vickers, J.A.; Caulum, M.M.; Henry, C.S. Generation of hydrophilic poly(dimethylsiloxane) for high-performance microchip electrophoresis. *Anal. Chem.* **2006**, *78*, 7446–7452, doi:10.1021/ac0609632.
43. Chen, I.J.; Lindner, E. The stability of radio-frequency plasma-treated polydimethylsiloxane surfaces. *Langmuir* **2007**, *23*, 3118–3122, doi:10.1021/la0627720.
44. Béfhay, S.; Lipnik, P.; Pardoen, T.; Nascimento, C.; Patris, B.; Bertrand, P.; Yunus, S. Thickness and elastic modulus of plasma treated PDMS silica-like surface layer. *Langmuir* **2010**, *26*, 3372–3375, doi:10.1021/la903154y.
45. Bar, G.; Delineau, L.; Häfele, A.; Whangbo, M.H. Investigation of the stiffness change in, the indentation force and the hydrophobic recovery of plasma-oxidized polydimethylsiloxane surfaces by tapping mode atomic force microscopy. *Polymer (Guildf)*. **2001**, *42*, 3627–3632, doi:10.1016/s0032-3861(00)00738-2.
46. Schneider, C.A.; Rasband, W.S.; Eliceiri, K.W. NIH Image to ImageJ: 25 years of image analysis. *Nat. Methods* **2012**, *9*, 671–675.
47. Mondal, P.; Rai, V.N.; Srivastava, A.K. A study of growth and thermal dewetting behavior of ultra-thin gold films using transmission electron microscopy. *AIP Adv.* **2017**, *075303*, doi:10.1063/1.4989823.
48. Zaporojtchenko, V.; Strunskus, T.; Behnke, K.; Bechtolsheim, C. V.; Thran, A.; Faupel, F. Formation of metal-polymer interfaces by metal evaporation: Influence of deposition parameters and defects. *Microelectron. Eng.* **2000**, *50*, 465–471, doi:10.1016/S0167-9317(99)00316-0.
49. Heni, W.; Vonna, L.; Fioux, P.; Vidal, L.; Haidara, H. Ultrasonic cavitation test applied to thin metallic films for assessing their adhesion with mercaptosilanes and surface roughness. *J. Mater. Sci.* **2014**, *49*, 6750–6761, doi:10.1007/s10853-014-8369-y.

50. Burkstrand, J.M. Metal-polymer interfaces: Adhesion and X-ray photoemission studies. *J. Appl. Phys.* **1981**, *52*, 4795.
51. Delcorte, A.; Befahy, S.; Poleunis, C.; Troosters, M. Improvement of metal adhesion to silicone films : a ToF-SIMS study. In *Adhesion Aspects of Thin Films*; Mittal, K.L., Ed.; 2005; Vol. 2, pp. 155–166.
52. Duguet, T.; Gavrielides, A.; Esvan, J.; Mineva, T.; Lacaze-Dufaure, C. DFT Simulation of XPS Reveals Cu/Epoxy Polymer Interfacial Bonding. *J. Phys. Chem. C* **2019**, *123*, 51.
53. Yu, S.; Sun, Y.; Ni, Y.; Zhang, X.; Zhou, H. Controlled Formation of Surface Patterns in Metal Films Deposited on Elasticity-Gradient PDMS Substrates. *ACS Appl. Mater. Interfaces* **2016**, *8*, 5706–5714, doi:10.1021/acsami.5b12369.
54. Haidara, H.; Papirer, Y.; Vallat, M.-F.; Schultz, J. Relationships between structural properties of vapour deposit metallic films on to polymer and their relevant adhesive performance. *J. Mater. Sci.* **1993**, *28*, 3243–3246.
55. Leosson, K.; Ingason, A.S.; Agnarsson, B.; Kossoy, A.; Olafsson, S.; Gather, M.C. Ultra-thin gold films on transparent polymers. *Nanophotonics* **2013**, *2*, 3–11, doi:10.1515/nanoph-2012-0030.
56. Zaporojtchenko, V.; Strunskus, T.; Behnke, K. Metal / polymer interfaces with designed morphologies. *J. Adhes. Sci. Technol.* **2000**, *14*, 467–490.
57. Bechtolsheim, C. V.; Zaporojtchenko, V.; Faupel, F. Interface structure and formation between gold and trimethylcyclohexane polycarbonate. *J. Mater. Res.* **1999**, *14*, 3538–3543, doi:10.1557/JMR.1999.0479.
58. Kiene, M.; Strunskus, T.; Peter, R.; Faupel, F. Evidence of aggregation-induced copper immobilization during polyimide metallization. *Adv. Mater.* **1998**, *10*, 1357–1360, doi:10.1002/(SICI)1521-4095(199811)10:16<1357::AID-ADMA1357>3.0.CO;2-9.
59. Kovacs, G.J.; Vincett, P.S. Formation and thermodynamic stability of a novel class of useful materials: Close-packed monolayers of submicron monodisperse spheres just below a polymer surface. *J. Colloid Interface Sci.* **1982**, *90*, 335–351, doi:10.1016/0021-9797(82)90302-2.
60. Thran, A.; Strunskus, T.; Zaporojtchenko, V.; Faupel, F. Evidence of noble metal diffusion in polymers at room temperature and its retardation by a chromium barrier. *Applied Phys. Lett.* **2002**, *14*, 1056.